Effect of Hydrocarbon Adsorption on the Wettability of Rare Earth Oxide Ceramics

Daniel J Preston[1], Nenad Miljkovic[1], Jean Sack[1], Ryan Enright[2], John Queeney[1], and Evelyn N Wang[1*]

[1]*Department of Mechanical Engineering, Massachusetts Institute of Technology, Cambridge, Massachusetts 02139, USA*
[2]*Thermal Management Research Group, Efficient Energy Transfer (ηET) Department, Bell Labs Ireland, Dublin 15, Ireland*

**Corresponding author email: enwang@mit.edu*

Abstract

Vapor condensation is routinely used as an effective means of transferring heat, with dropwise condensation exhibiting a 5 – 7x heat transfer improvement compared to filmwise condensation. However, state-of-the-art techniques to promote dropwise condensation rely on functional hydrophobic coatings, which are often not robust and therefore undesirable for industrial implementation. Natural surface contamination due to hydrocarbon adsorption, particularly on noble metals, has been explored as an alternative approach to realize stable dropwise condensing surfaces. While noble metals are prohibitively expensive, the recent discovery of robust rare earth oxide (REO) hydrophobicity has generated interest for dropwise condensation applications due to material costs approaching 1% of gold; however, the underlying mechanism of REO hydrophobicity remains under debate. In this work, we show through careful experiments and modeling that REO hydrophobicity occurs due to the same hydrocarbon adsorption mechanism seen previously on noble metals. To investigate adsorption dynamics, we studied holmia and ceria REOs, along with control samples of gold and silica, *via* X-Ray photoelectron spectroscopy (XPS) and dynamic time-resolved contact angle measurements. The contact angle and surface

carbon percent started at ≈ 0 on in-situ argon-plasma-cleaned samples and increased asymptotically over time after exposure to laboratory air, with the rare earth oxides displaying hydrophobic (> 90 degrees) advancing contact angle behavior at long times (> 4 days). The results indicate that REOs are in fact hydrophilic when clean, and become hydrophobic due to hydrocarbon adsorption. Furthermore, this study provides insight into how REOs can be used to promote stable dropwise condensation, which is important for the development of enhanced phase change surfaces.

KEYWORDS: Condensation, Dropwise, Hydrocarbon adsorption, Rare earth oxide, Wettability

Condensation is observed frequently in our environment and routinely used in industry as an effective means of transferring heat. Water condensation on typical industrial condenser metal surfaces and their respective high-surface-energy oxides, *e.g.*, CuO, Al_2O_3, and Fe_2O_3, results in the formation of a film of condensate that spreads over the condenser surface, termed filmwise condensation.[1] This filmwise mode of condensation imposes a thermal resistance across the film, which limits heat transfer. Conversely, water condensation on a low-surface-energy material, *e.g.*, PTFE, parylene, and PFDA, results in the formation of discrete condensate droplets that, when under gravity-driven convection, shed as their size approaches the capillary length (≈2 mm for water), termed dropwise condensation.[2] The shedding of droplets refreshes the surface for renucleation and offers an improvement in heat transfer performance of 5 – 7x compared to filmwise condensation.[3]

State-of-the-art techniques to promote dropwise condensation rely on the application of low-surface-energy hydrophobic coatings to the condenser surface.[3,4] Coatings as thin as a monolayer (≈1 nm) of long-chain fluorocarbon molecules or fatty acids can be applied to induce hydrophobicity, but these are often not robust over extended periods of time and therefore unsuitable in industrial applications.[5] Thicker polymer coatings, *e.g.*, ≈ 20 μm coating of PTFE, have shown the potential to maintain robust hydrophobicity, but have a characteristically large thermal resistance that can negate the advantage gained by achieving dropwise condensation.[3] More recently, plasma enhanced chemical vapor deposition (PECVD) and initiated chemical vapor deposition (iCVD) have been used to grow ultra-thin (< 40 nm) conformal coatings of polymer on surfaces with success in achieving dropwise condensation.[5,6] However, the longevity of these ultra-thin coatings remains a question due to the lack of extended or accelerated testing to assess mechanical durability and long-term stability.

An alternative to the direct application of low-surface-energy coatings relies on surface contamination due to energetically favorable hydrocarbon adsorption, particularly on high thermal conductivity noble metals (*i.e.*, gold and silver).[7] These metals are wetting when clean, but reduce their surface energy by adsorbing hydrocarbons from air, enabling dropwise condensation when used as condenser surfaces. The robustness of this approach is well-documented, with one paper demonstrating continuous dropwise condensation on gold for over five years in a closed system.[8] Unfortunately, the high price of noble metals prohibits this approach in practice.

Researchers have recently demonstrated rare earth oxides (REOs) as potential candidates for condenser surface coatings due the their apparent intrinsic hydrophobicity[9] and costs approaching 1% of gold.[10] However, reported contact angles on REOs are inconsistent.

Advancing contact angles ranging from 17 – 134° have been observed, with a study reporting 94 - 134° on rough electroplated ceria coatings[11]. Meanwhile another study reports 120° on a rough ceria membrane, but 17° on ceria after oxidation by heating cerium foil in air and 31° on a rough ceria membrane which has been sonicated in ethanol to destroy the nanostructure.[12]

Furthermore, the underlying mechanism of REO hydrophobicity does not seem to be well-understood. The initially reported intrinsic hydrophobicity of REOs asks for a comparison with the debate in scientific literature regarding the intrinsic wettability of gold in the 1960s.[9] Erb and Fowkes asserted that gold was intrinsically hydrophobic in 1964,[8,13] which Zisman contradicted the following year with experiments demonstrating that the contact angle on a gold surface with hydrocarbons desorbed and oxide removed (by heating in a hydrogen gas stream with < 1ppm hydrocarbons) was ≈ 0°.[14] Though Erb initially disputed the claim,[15] subsequent studies determined that gold is intrinsically hydrophilic but rapidly adsorbs hydrocarbons from the ambient environment, resulting in an increased contact angle.[16] The idea of achieving hydrophobicity *via* hydrocarbon adsorption has been extended for a wide class of materials, including ceramic metal oxides[17,18] as well as pristine monolayer graphene.[19] However, in the case of REOs such as ceria, while previous work has shown that methane adsorbs to the surface[20] and hydrocarbon adsorption increases on roughened surfaces with more available surface area,[21] adsorption of hydrocarbons besides methane and the subsequent effect on contact angle have not been investigated. In this work, we show through experiments and modeling that REO hydrophobicity occurs due to a similar hydrocarbon adsorption mechanism observed previously on noble metals. To investigate adsorption dynamics under ambient conditions, we studied two REOs with different oxidation states, holmia (Ho_2O_3) and ceria (CeO_2), along with control

samples of silica on a silicon wafer substrate and gold; both chosen because literature values on the effect of hydrocarbon adsorption were readily available.

REO samples were fabricated by pressing and sintering powders (Sigma-Aldrich: holmia, 99.9% pure, 100 nm; ceria, 99.9% pure, 5 μm) in accordance with the procedure described in the study which first reported REO hydrophobicity.[9] First, the powders were dry-pressed into ≈ 2 mm thick chips at 270 MPa and then at 350 MPa in a 13-mm-diameter steel pellet die (REFLEX evacuable pellet die). The chips were then sintered for 4 hr at 1600 °C and 1560 °C for holmia and ceria, respectively, in a box furnace (Blue-M, Thermo Scientific). Field emission scanning electron microscopy images of the grains formed during sintering are shown in Figure 1 along with atomic force microscopy (AFM) scans of the surface. The surface roughness, defined as the ratio of actual surface area to projected surface area, was determined from AFM to be less than 1.05 for both samples, which indicates that surface roughness did not significantly impact wettability.

To ensure a pristine surface, the samples were cleaned with argon plasma (Harrick PDC-001) until no contaminants were present as evidenced by X-ray photoelectron spectroscopy (XPS) (Thermo Scientific K-Alpha), and the samples were further bombarded by argon ions inside of the XPS chamber before the first (pristine) measurement of surface composition. Argon plasma was used because it is inert and removes contamination by physical bombardment as compared to oxygen-containing plasma, which reacts chemically with the surface.[22] Furthermore, argon plasma has been shown to remove adsorbed hydrocarbons and does not significantly increase surface roughness.[23] The pristine surfaces after argon ion bombardment showed that the surfaces exhibited the expected stoichiometric ratios for their respective oxidation states, with gold in its elemental state (Table I).

After cleaning, the samples were exposed to laboratory air (MIT Rohsenow-Kendall Heat Transfer Laboratory, ambient temperature = 25 ± 2 °C, relative humidity = 35 ± 10%) and the advancing and receding contact angles and XPS spectra were measured at multiple time points. Contact angles were obtained by microgoniometric measurement (Kyowa MCA-3, see supplementary Figure S2[24]). Droplet vibrations induced by the piezoelectric dispenser head[25] did not affect the measurements.[24] The advancing and receding contact angles are presented as opposed to the equilibrium contact angle to thoroughly describe the surface wettability[26] and to characterize the force needed to hold the droplet stationary on an inclined condensing surface against the force of gravity, which directly affects condensation heat transfer (see supplementary material).[24] To determine the amount of adsorbed hydrocarbon, the surface carbon percent was measured from the relative peak magnitudes of the surface components observed from XPS spectra taken at each time point. Representative XPS spectra for holmia and ceria are presented in Figure 2. Comparison between the XPS spectra for pristine holmia and ceria and at 96 hours after cleaning reveals that a sharp carbon peak develops, often referred to as the "adventitious carbon" peak, which is indicative of adsorption of hydrocarbons onto the surface.[27] Note that hydrogen cannot be explicitly detected by XPS because it only has valence electrons, which are indistinguishable from other elements upon excitation and for which the binding energy is influenced by environment; therefore, determination of the average hydrocarbon chain length was not possible.[28]

The average advancing contact angle measurements for each sample as a function of time after argon plasma cleaning started at ≈ 0° and increased asymptotically over time for every sample (Fig. 3), with the REO's displaying hydrophobic ($\theta_a > 90°$) behavior after 4 days. Note that both the advancing and receding angles for all of the surfaces except gold were less than 10°

immediately after cleaning, and, as a result, the contact angle hysteresis was also initially less than 10° (the advancing/receding contact angles on gold were 46°/10° at the time of the first measurement). At 2448 hours (102 days) after cleaning, the average advancing angle reached 103° for holmia and 95° for ceria, which are within 10% of the previously reported values.[9] The advancing angles on gold and silicon reached 66° and 44°, respectively, which are in good agreement with the literature values for hydrocarbon contamination of these surfaces after cleaning to their pristine state and exposing to laboratory air.[8,15,29] Representative images of the advancing contact angle increase over time on the REOs are shown in Figure 3(b, c).

The increase in advancing contact angle over time suggests that the surface energy decreases over time, which can be attributed to the lower surface energy of the adsorbed hydrocarbons.[30] This trend has been previously shown for a variety of non-noble metal oxide materials including zirconium dioxide (ZrO_2) and titanium dioxide (TiO_2), among others, and occurs due to physisorption of hydrocarbons to OH^- groups and other energetically favorable sites present on the surface,[17,31] where van-der-Waals and hydrogen bonding are typical[32] but covalent bonding is also possible.[33] The results of the XPS analysis conducted here show that the amount of carbon present on the surface is indeed increasing over time, indicating that hydrocarbons adsorb to the cleaned surface after exposure to air. As shown in Figure 4a, the surface atomic percent of carbon increased from ≈ 0% immediately after cleaning to an asymptotic value of between 12 – 34% depending on sample type.

To explore the relationship between advancing contact angle and hydrocarbon adsorption, the measured advancing and receding angles are shown as a function of the surface atomic percent carbon for holmia and ceria in Figure 4(b, c). The advancing and receding contact angles increased with surface atomic percent carbon, where the advancing and receding

contact angles are positively correlated with surface atomic percent carbon with a Pearson product-moment of at least 0.93 for all of the samples studied here. This is in agreement with previous work for metals and metal oxides (see supplementary Figure S3).[24] The mechanism for this relationship can be explained by considering the adsorbed hydrocarbons to be hydrophobic defects on an initially hydrophilic surface.[34] If the hydrocarbons are approximated as circular hydrophobic defects, then the advancing angle is predicted by:

$$\cos(\theta_A) = f_{max}\cos\left(\theta_{1,A}\right) + (1 - f_{max})\cos\left(\theta_{2,A}\right), \quad (1)$$

where θ_A is the advancing contact angle as a function of the surface coverage of hydrocarbons, f_{max}, which is determined from the surface atomic percent carbon and the relative sizes of the adsorbed hydrocarbons and the surface atoms, $\theta_{1,A}$ is the advancing contact angle of the hydrophilic surface with no adsorbed hydrocarbons ($\approx 0°$), and $\theta_{2,A}$ is the advancing contact angle on the surface once it has become saturated with hydrocarbons (approximated as the advancing angle at 2448 hours) (See expanded explanation in supplementary material[24]). The curve obtained from this model is shown to fit well with the experimental data, indicating that hydrocarbon adsorption results in the observed increase contact angle. Modeling the receding angle in this case yields less useful information due to adhesion hysteresis of the adsorbed hydrocarbons and the variability in receding behavior as a function of time that the droplet remains on the surface.[35]

This work demonstrates that the hydrophobicity of REOs is due to hydrocarbon adsorption, as shown by the relationship between the increasing contact angle and surface carbon percent over time upon exposing a pristine surface to atmosphere. Similar to the noble metals and more typical metal oxides, pristine REOs have high surface energy, making them intrinsically hydrophilic. This study on the evolution in wetting behavior suggests that REOs can

serve as coatings to induce dropwise condensation for improved heat transfer performance through the spontaneous adsorption of hydrocarbon material and subsequent effect on wetting behavior.

The potential of REOs as functional surface coatings for condensers due to their hydrophobicity after hydrocarbon adsorption is promising, but also raises concerns. The large contact angle hysteresis of the REO surfaces studied here (~60° – 70°), and shown previously,[9] will act to increase the size of departing droplets, which negatively impacts heat transfer.[3] Another challenge is the thermal expansion coefficient mismatch between REOs (4 – 10 μm/m-K) and many industrial condenser metals (10 – 25 μm/m-K), which could result in fracturing of thin and brittle REO coatings due to temperature fluctuations.[36] However, the relatively low cost and moderate thermal conductivities of REOs (2.4 – 13.3 W/m-K, see supplementary material[24]) offer a potentially unique advantage over traditional promoter coatings. Layers of hydrophobic polymers (PTFE) have been shown to give excellent dropwise condensation behavior but have only been found to be sufficiently durable when the thickness (δ) of the low-conductivity polymer (k_p ~ 0.2 W/m·K) layer is so large ($\delta_p \approx 20$ μm) as to offset the advantage of dropwise condensation.[37] The larger coating thickness is typically required in order to increase adhesion to the metal substrate and enhance resistance to oxidation and moisture. Gold coatings have been shown to give excellent dropwise condensation but have only been found to be sufficiently durable (≈5.7 years of operating time) when the thickness of the gold is so large (≈50 μm) as to make the approach economically unfeasible.[38] On the other hand, REOs strike a balance between the two previous approaches in terms of cost and thermal conductivity. The moderate thermal conductivity of REOs allows for a ~25*x* thicker coating than conventional polymer layers while maintaining a comparable thermal resistance with the added benefit of

potentially greater adhesion and durability.[9] Furthermore, the reduced cost of REOs compared to gold coatings makes their application to industrial materials more economically feasible.[39] In the future, more rigorous calculations of the expected condensation heat transfer are needed based on existing high fidelity models in the literature.[3,40]

This study provides insight on the wetting mechanism of the REO material group that suggests potential for implementation in other fields which make use of hydrophobic materials, including self-cleaning surfaces,[41] anti-icing surfaces,[42] water desalination,[43] and enhanced heat transfer surfaces.[4,44] Furthermore, our work highlights the importance of controlling hydrocarbon adsorption for material wetting characterization.

Acknowledgements

We thank Dr. Jay J. Senkevich of MIT for fruitful discussions regarding hydrocarbon adsorption. We gratefully acknowledge funding support from the Office of Naval Research (ONR) with Dr. Mark Spector as program manager and the MIT S3TEC Center, an Energy Frontier Research Center funded by the Department of Energy, Office of Science, Basic Energy Sciences, under Award DE-FG02-09ER46577. D. J. Preston acknowledges funding received by the National Science Foundation Graduate Research Fellowship under Grant No. 1122374. Any opinion, findings, conclusions, or recommendations expressed in this material are those of the authors(s) and do not necessarily reflect the views of the National Science Foundation. R. Enright acknowledges funding received from the Irish Research Council for Science, Engineering, and Technology, cofunded by Marie Curie Actions under FP7. Bell Labs Ireland thanks the Industrial Development Agency (IDA) Ireland for their financial support. We also acknowledge the support from the National Science Foundation through the Major Research Instrumentation Grant for Rapid Response Research (MRI-RAPID) for the microgoniometer. This work was

performed in part at the Center for Nanoscale Systems (CNS), a member of the National Nanotechnology Infrastructure Network (NNIN), which is supported by the National Science Foundation under NSF award no. ECS-0335765. CNS is part of Harvard University.

References

[1] W. Nusselt, Z Ver Dtsch Ing **60**, 541 (1916).

[2] E. Schmidt, W. Schurig, and W. Sellschopp, Z Ver Dtsch Ing **74**, 544 (1930).

[3] J. W. Rose, P I Mech Eng a-J Pow **216** (A2), 115 (2002).

[4] R. Enright, N. Miljkovic, J. L. Alvarado, K. J. Kim, and J.W. Rose, Nanoscale and Microscale Thermophysical Engineering (2014).

[5] A. T. Paxson, J. L. Yague, K. K. Gleason, and K. K. Varanasi, Adv Mater (2013).

[6] N. Miljkovic, D. J. Preston, R. Enright, and E. N. Wang, Nat Commun **4** (2013).

[7] F. E. Bartell and P. H. Cardwell, J Am Chem Soc **64**, 494 (1942).

[8] R. A. Erb, J Phys Chem-Us **69** (4), 1306 (1965).

[9] G. Azimi, R. Dhiman, H. M. Kwon, A. T. Paxson, and K. K. Varanasi, Nat Mater **12** (4), 315 (2013).

[10] Cost data for gold obtained from money.cnn.com and for holmia and ceria from sigmaaldrich.com referenced February 2014.

[11] L. Martinez, E. Roman, J. L. de Segovia, S. Poupard, J. Creus, and F. Pedraza, Appl Surf Sci **257** (14), 6202 (2011).

[12] N. J. Lawrence, K. Jiang, and C. L. Cheung, Chemical Communications **47** (9), 2703 (2011).

[13] F. M. Fowkes, Ind Eng Chem **56** (12), 40 (1964).

[14] K. W. Bewig and W. A. Zisman, J Phys Chem-Us **69** (12), 4238 (1965).

[15] R. A. Erb, Journal of Physical Chemistry **72** (7), 2412 (1968).

[16] M. K. Bernett and W. A. Zisman, J Phys Chem-Us **74** (11), 2309 (1970); M. E. Schrader, J Phys Chem-Us **84** (21), 2774 (1980); T. Smith, J Colloid Interf Sci **75** (1), 51 (1980); M. Schneegans and E. Menzel, J Colloid Interf Sci **88** (1), 97 (1982); G. L. Gaines, J Colloid Interf Sci **79** (1), 295 (1981); M. E. Schrader, J Colloid Interf Sci **100** (2), 372 (1984).

[17] S. Takeda, M. Fukawa, Y. Hayashi, and K. Matsumoto, Thin Solid Films **339** (1-2), 220 (1999).

[18] B. R. Strohmeier, J Vac Sci Technol A **7** (6), 3238 (1989).

[19] Z. T. Li, Y. J. Wang, A. Kozbial, G. Shenoy, F. Zhou, R. McGinley, P. Ireland, B. Morganstein, A. Kunkel, S. P. Surwade, L. Li, and H. T. Liu, Nat Mater **12** (10), 925 (2013).

[20] L. Can and X. Qin, J Phys Chem-Us **96** (19), 7714 (1992).

[21] Hyuk-Min Kwon, Massachusetts Institute of Technology, 2013.

[22] R. Nickerson, Polymers, Laminations & Coatings Conference, Books 1 and 2, 1101 (1998).

[23] A. L. Sumner, E. J. Menke, Y. Dubowski, J. T. Newberg, R. M. Penner, J. C. Hemminger, L. M. Wingen, T. Brauers, and B. J. Finlayson-Pitts, Phys Chem Chem Phys **6** (3), 604 (2004); A. Wasy, G. Balakrishnan, S. H. Lee, J. K. Kim, D. G. Kim, T. G. Kim, and J. I. Song, Crystal Research and Technology **49** (1), 55 (2014); I. Umezu, K. Kohno, K. Aoki, Y. Kohama, A. Sugimura, and M. Inada, Vacuum **66** (3-4), 453 (2002).

[24] See supplementary material at (web address) for additional information on characterization methods; detailed description of the contact angle model; tabulated REO thermal conductivities; and supplementary figures.

[25] E. Bormashenko, R. Pogreb, G. Whyman, and M. Erlich, Langmuir **23** (24), 12217 (2007); E. Bormashenko, R. Pogreb, G. Whyman, Y. Bormashenko, and M. Erlich, Appl Phys Lett **90** (2007); X. Noblin, A. Buguin, and F. Brochard-Wyart, Eur Phys J E **14** (4), 395 (2004).

[26] L. C. Gao and T. J. McCarthy, Langmuir **25** (24), 14105 (2009); L. C. Gao and T. J. McCarthy, Langmuir **22** (14), 6234 (2006).

[27] T. L. Barr and S. Seal, J Vac Sci Technol A **13** (3), 1239 (1995).

[28] N. Stojilovic, J Chem Educ **89** (10), 1331 (2012).

[29] R. R. Thomas, F. B. Kaufman, J. T. Kirleis, and R. A. Belsky, J Electrochem Soc **143** (2), 643 (1996).

[30] D. L. Katz and W. Saltman, Ind Eng Chem **31**, 91 (1939).

[31] W. Birch, A. Carre, and K. L. Mittal, Dev Surf Contam Cl **1**, 693 (2008).

[32] S. N. Lanin, D. A. Pichugina, A. F. Shestakov, V. V. Smirnov, S. A. Nikolaev, K. S. Lanina, A. Y. Vasil'kov, F. T. Zung, and A. V. Beletskaya, Russ J Phys Chem a+ **84** (12), 2133 (2010).

[33] J. H. Kim, J. Jung, K. Tahara, Y. Tobe, Y. Kim, and M. Kawai, J Chem Phys **140** (7) (2014); G. Jones, F. Studt, F. Abild-Pedersen, J. K. Norskov, and T. Bligaard, Chem Eng Sci **66** (24), 6318 (2011); V. A. Rigo, C. O. Metin, Q. P. Nguyen, and C. R. Miranda, J Phys Chem C **116** (46), 24538 (2012).

[34] R. Raj, R. Enright, Y. Y. Zhu, S. Adera, and E. N. Wang, Langmuir **28** (45), 15777 (2012).

[35] Y. L. Chen, C. A. Helm, and J. N. Israelachvili, J Phys Chem-Us **95** (26), 10736 (1991).

[36] H. Singh and B. Dayal, Journal of the Less Common Metals **18** (2), 172 (1969); M. Gupta and S. Singh, J Am Chem Soc **53** (12), 663 (1970).

[37] P. J. Marto, D. J. Looney, J. W. Rose, and A. S. Wanniarachchi, Int J Heat Mass Tran **29** (8), 1109 (1986).

[38] RobertA Erb, Gold Bull **6** (1), 2 (1973).

[39] D. W. Woodruff and J. W. Westwater, Int J Heat Mass Tran **22** (4), 629 (1979).

[40] J. W. Rose, Int J Heat Mass Tran **24** (2), 191 (1981); Nenad Miljkovic, Ryan Enright, and Evelyn N. Wang, Journal of Heat Transfer **135** (11), 111004 (2013); S. Kim and K. J. Kim, Journal of Heat Transfer **133** (8), 081502 (2011).

[41] K. M. Wisdom, J. A. Watson, X. P. Qu, F. J. Liu, G. S. Watson, and C. H. Chen, P Natl Acad Sci USA **110** (20), 7992 (2013).

[42] L. L. Cao, A. K. Jones, V. K. Sikka, J. Z. Wu, and D. Gao, Langmuir **25** (21), 12444 (2009); L. Mishchenko, B. Hatton, V. Bahadur, J. A. Taylor, T. Krupenkin, and J. Aizenberg, Acs Nano **4** (12), 7699 (2010).

[43] T. Humplik, J. Lee, S. C. O'Hern, B. A. Fellman, M. A. Baig, S. F. Hassan, M. A. Atieh, F. Rahman, T. Laoui, R. Karnik, and E. N. Wang, Nanotechnology **22** (29) (2011); A. D. Khawaji, I. K. Kutubkhanah, and J. M. Wie, Desalination **221** (1-3), 47 (2008).

[44] N. Miljkovic and E. N. Wang, Mrs Bull **38** (5), 397 (2013).

Figures and Tables

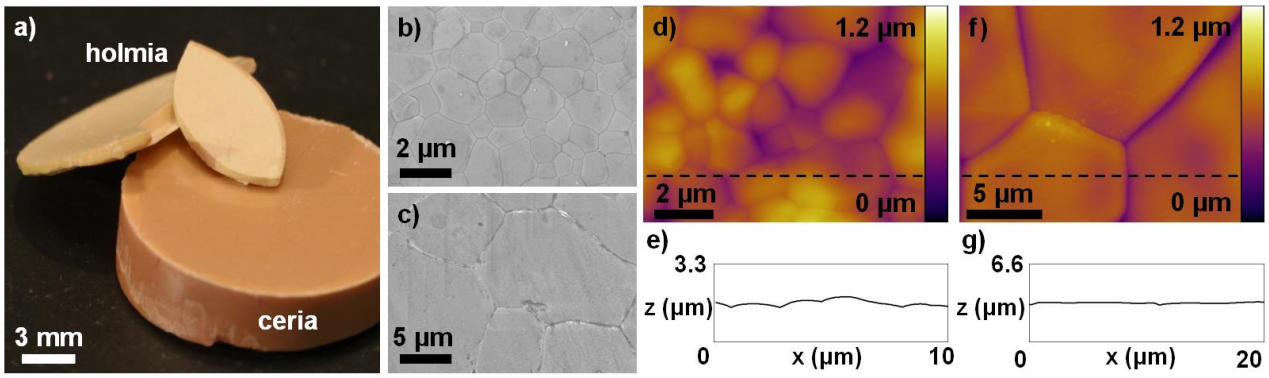

Figure 1. (Double Column, AR = 3.40)

Table 1. (Single Column)

Sample	Element	Atomic %	Element	Atomic %
Holmia (Ho_2O_3)	Ho	41	O	59
Ceria (CeO_2)	Ce	33	O	67
Silica (SiO_2)	Si	34	O	66
Gold (Au)	Au	100	-	-

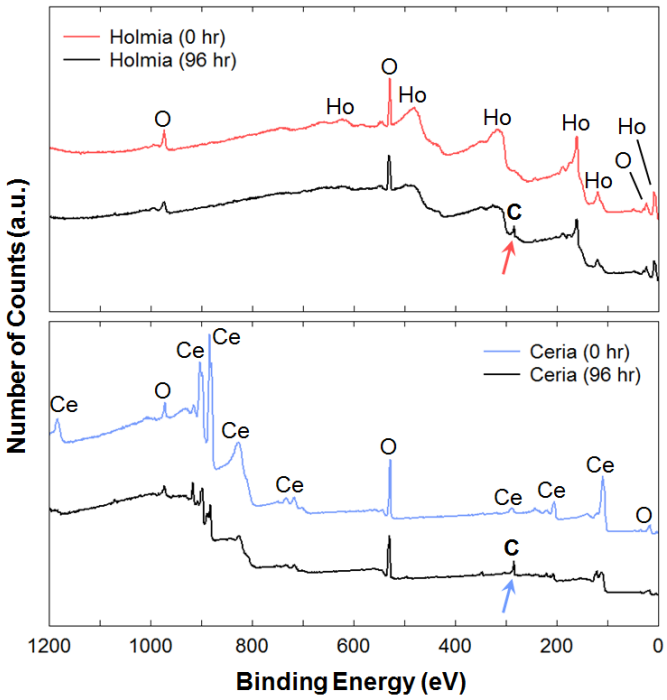

Figure 2. (Single Column, AR = 0.95)

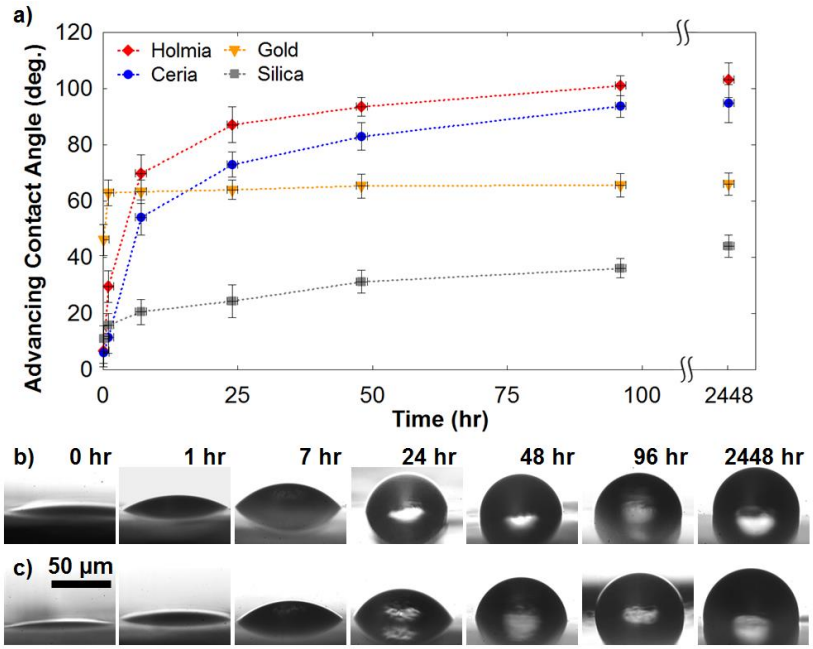

Figure 3. (Single Column, AR = 1.25)

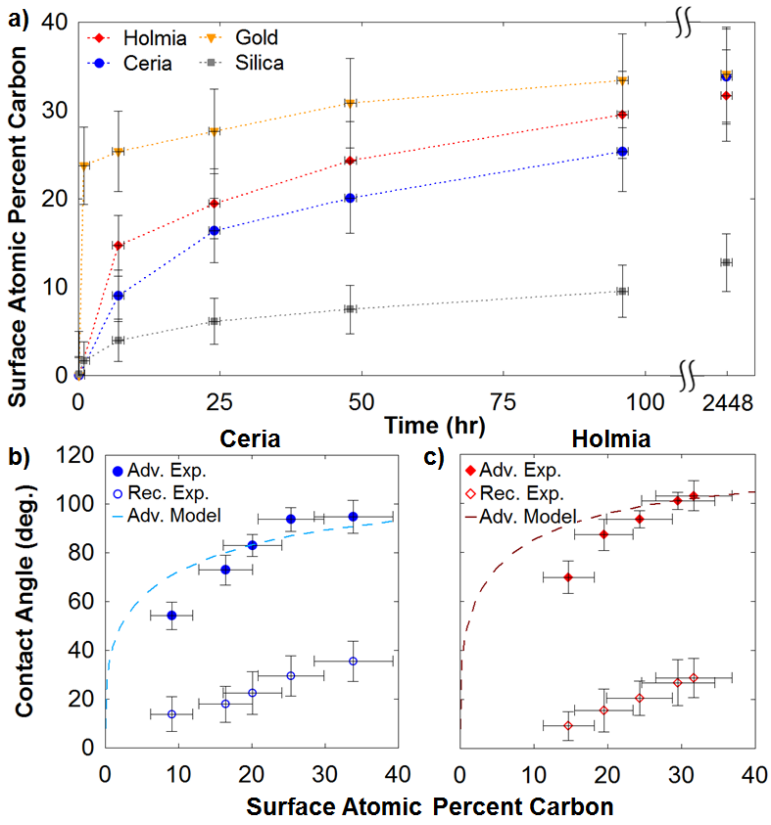

Figure 4. (Single Column, AR = 0.95)

Figure and table captions

Figure 1. (a) Holmia (Ho_2O_3) and ceria (CeO_2) samples after dry-pressing and sintering. The holmia fracture shows the brittle nature of the REOs. Field emission scanning electron microscopy images are shown for the (b) holmia and (c) ceria surfaces. The average grain sizes are ≈1 μm and ≈10 μm, respectively. AFM scans of the surfaces are presented here with height profiles along the dashed lines on these scans shown below for (d and e) holmia and (f and g) ceria. The ratio of actual surface area to projected surface area was measured to be less than 1.05 for both REO samples.

Table 1. Elements present on pristine REO (ceria and holmia) and control (silica and gold) surfaces in stoichiometric ratios after cleaning by bombardment with argon ions; atomic percent determined by XPS.

Figure 2. Survey XPS spectra of (a) holmia and (b) ceria immediately after argon ion bombardment (0 hr) and after 4 days exposed to laboratory air (96 hr). For both REOs, sharp carbon peaks developed by 96 hr which were not present at 0 hr, indicated here with arrows, which confirm the adsorption of hydrocarbons on the surface. The 0 hr spectra were shifted upwards by a constant value for comparison between spectra.

Figure 3. (a) Average advancing contact angle as a function of time for the REO (holmia and ceria) and control (gold and silica) samples exposed to laboratory air (temperature ≈ 25 °C, relative humidity ≈ 35%) with t=0 at the instant of argon ion bombardment surface cleaning. The average contact angle, defined as the mean of the contact angles measured on at least 5 spots on each sample, increased asymptotically with time for each sample. The error bars for the average contact angle range from 3-7° due to error in the measurement and variance between data points. Representative time-lapse images of advancing contact angles observed *via* microgoniometer are shown for (b) holmia and (c) ceria samples.

Figure 4. (a) Surface atomic percent carbon as a function of time for the REO and control samples exposed to laboratory air (temperature ≈ 25 °C, relative humidity ≈ 35%) with t = 0 at the instant of argon ion bombardment surface cleaning. Surface atomic percent carbon was calculated based on the relative peak sizes from XPS spectra taken at each data point and increased asymptotically with time. The error bars for surface atomic percent carbon range from 15-30% of the values shown due to error in the XPS measurement and the calculation of atomic percent from the spectra. The contact angle is shown as a function of surface carbon percent for (b) ceria and (c) holmia, and the advancing angle agrees well with a theoretical curve calculated from a model prediction accounting for hydrocarbons on a hydrophilic surface.

Effect of Hydrocarbon Adsorption on the Wettability of Rare Earth Oxide Ceramics

Supplementary Material

Daniel J Preston[1], Nenad Miljkovic[1], Jean Sack[1], Ryan Enright[2], John Queeney[1], and Evelyn N Wang[1*]

[1]*Department of Mechanical Engineering, Massachusetts Institute of Technology, Cambridge, Massachusetts 02139, USA*
[2]*Thermal Management Research Group, Efficient Energy Transfer (ηET) Department, Bell Labs Ireland, Dublin 15, Ireland*

**Corresponding author email: enwang@mit.edu*

Characterization Methods

The field emission scanning electron microscope used to capture the images in Figure 1 was an Ultra Plus (Carl Zeiss AG). The in-lens detector was used to image the samples at a voltage of 2.00 kV. The samples were mounted to stubs with carbon tape and were not used for experimental results after imaging.

The AFM scans in Figure 1 were obtained with an Asylum MFP-3D using Bruker TESP probes. The scan rate was 5 μm/sec, and the scan area was 10 μm x 10 μm for the holmia sample and 20 μm x 20 μm for the ceria sample. The samples were not used for experimental results after the AFM scans were conducted.

The XPS spectra were obtained with a Thermo Scientific K-Alpha XPS. The measurements were performed with a 400 μm X-ray spot size at pressures less than $8x10^{-8}$ mBar. The spectra were post-processed with Advantage software (version 5.918) to determine the initial composition of the pristine samples and the surface atomic percent carbon at each time point from relative peak heights.

Contact angles were obtained with a Kyowa MCA-3 microgoniometer with a piezoelectric head to dispense picoliter-scale droplets at frequencies of 20 – 1000 Hz. The average advancing angle data was obtained by taking the mean of the advancing contact angles measured on at least 5 spots on each sample for each time point. The average receding contact angle was obtained by the same method, and was observed when the droplet contact line receded during evaporation of the droplet. See Figure S2 for the measured contact angle during the advancing and receding phases for a representative sample (holmia, 2448 hr after plasma cleaning process).

Advancing Contact Angle Model

The hydrocarbon adsorption phenomenon was modeled as hydrophobic defects on an initially hydrophilic surface to predict the advancing contact angle. Approximating the hydrocarbons as circular hydrophobic defects on the surface, the advancing angle is predicted by:

$$\cos(\theta_A) = f_{max}\cos\left(\theta_{1,A}\right) + (1 - f_{max})\cos\left(\theta_{2,A}\right), \quad (1)$$

where θ_A is the advancing contact angle as a function of the surface coverage of hydrocarbons, $\theta_{1,A}$ is the advancing contact angle of the hydrophilic surface with no adsorbed hydrocarbons ($\approx 0°$), and $\theta_{2,A}$ is the advancing contact angle on the surface once it has become saturated with hydrocarbons (approximated as the advancing angle at 2448 hours). The term f_{max} represents the surface area coverage of hydrophobic defects at the region where the energy barrier to advance is highest; in the case of uniform circular defects, this is the ratio of the diameter of a circular hydrophobic defect, *D*, to the side length of the square area surrounding each circular defect, *L*. Since the XPS spectra provide the surface atomic percent carbon and not the area coverage, the surface atomic percent carbon is converted to a ratio of hydrocarbon-covered surface area to total surface area, which is then used to determine $f_{max} = D/L$ and $\theta_A = \theta_A(f_{max})$.

To convert surface atomic percent carbon to percent hydrocarbon-covered surface area, the area ratio of the hydrocarbon molecules on the surface to the adsorbent surface molecules is required. This is approximated from the molar specific volumes as:

$$A_{HC}/A_M = (V_{HC}/V_M)^{2/3}, \quad (S1)$$

where the subscript *HC* indicates hydrocarbons and the subscript *M* indicates the adsorbent surface molecules. The molar specific volume for methane was used in this analysis in order to assign one mole of hydrocarbon to every adsorbed carbon atom while maintaining a good estimate for hydrocarbon surface area. The fraction of hydrocarbon-covered surface area is then calculated as:

$$A_{HC}/A_{total} = (1 + (A_{HC}/A_M)(1 - C)/(C))^{-1}, \quad (S2)$$

where *C* is the surface percent carbon by mole , which is obtained from the raw XPS surface atomic percent carbon by accounting for the number of atoms per molecule based on the unit molecules for which the molar specific volumes were obtained. Finally, f_{max} is calculated as:

$$f_{max} = \sqrt{(4/\pi)(A_{HC}/A_{total})} \quad (S3)$$

The curve obtained from this model is shown to match well with the experimental data, indicating that hydrocarbon adsorption is a plausible mechanism for the observed increase in contact angle.

Rare Earth Oxide Thermal Conductivities

The thermal conductivities (k) for selected REOs are shown in Table S1. The calculated values were determined from known values for the density (ρ), heat capacity (C_p), and thermal diffusivity (α) of the REOs ($k = \alpha\rho C_p$). The experimentally measured values were obtained from literature.

Table S1. Thermal conductivities of selected REOs.

Element	Atomic #	Oxidation State	Thermal Cond., k_{calc} [W/m·K]	Thermal Cond., k_{exp} [W/m·K]
Yttrium	39	Y_2O_3	12.77	13.3[1]
Lanthanum	57	La_2O_3	5.88	6.0[2]
Cerium	58	CeO_2	-	11.7[1,3]
Samarium	62	Sm_2O_3	15.42	9.7[1]
Europium	63	EuO	-	7.0[4]
Europium	63	Eu_2O_3	2.33	2.4[5]
Gadolinium	64	Gd_2O_3	12.21	10.3[1]
Lutetium	71	Lu2O3	12.42	-

Comparison of Coating Thicknesses

To maintain the same thermal resistance for the coating, comparing REOs (taking a conservative thermal conductivity value of $k_{REO} \approx 5$ W/m·K) to polymer coatings (thermal conductivity $k_p \approx 0.2$ W/m·K) and using the relationship $\delta_{REO} \sim (k_{REO}/k_p)\bullet\delta_p$, we find that the REO coating can be ~25x thicker with comparable thermal resistance, where δ_{REO} is the thickness of the REO coating and δ_p is the thickness of a polymer coating which would result in an equivalent thermal resistance.

Microgoniometer Piezoelectric Head Droplet Injection

The piezoelectric head is capable of dispensing picoliter-scale droplets at frequencies of 20 – 1000 Hz during microgoniometric measurement. The potential to introduce vibrations in the droplet being observed during advancing of the contact angle by dispensing droplets for the piezoelectric head, which may cause the contact line to oscillate, is considered here. First, the Ohnesorge number for a water droplet of the size observed during contact angle measurement (diameter $D \approx 50$ μm) is:

$$Oh = \frac{\mu}{\sqrt{\rho\sigma D}} \approx 0.01 \tag{S4}$$

where μ is water viscosity, ρ is water density, and σ is water surface tension at room temperature. Therefore, viscous effects are neglected and a balance between inertial and surface tension forces is considered. Determining the droplet natural frequency for the first resonant mode in this case[6]:

$$f = \frac{1}{2\pi}\sqrt{\frac{6\sigma h(\theta)}{\rho(1-cos\theta)(2+cos\theta)}R^{-3/2}} \approx 6{,}000\ Hz \tag{S5}$$

where θ is the droplet contact angle on the surface a (90° was used as a representative value) and $h(\theta)$ is a factor which includes the dependence on geometry.[7] The experimental data points were obtained with droplet dispensing frequencies of 20 – 40 Hz << 6,000 Hz (1,000 Hz droplet dispensing was used to align the camera, not for measurement); therefore, the resonant vibration modes of the droplet under observation were not activated and the contact line did not oscillate due to addition of picoliter-scale droplets, allowing for accurate measurement of the advancing contact angle during droplet dispensing.

Role of Advancing and Receding Contact Angle in Dropwise Condensation Performance

The contact angle hysteresis plays a large role in dropwise condensation, where the advancing and receding contact angles determine the force needed to hold a droplet stationary on an inclined condensing surface against the force of gravity. A typical scaling of maximum droplet size on a vertical condenser surface is obtained by balancing the droplet weight with the contact angle hysteresis force acting on the droplet, as shown in Equation S6, where it is observed that the advancing and receding contact angles provide valuable information about the expected droplet departure size while the equilibrium contact angle is unable to provide this information. The maximum droplet departure size directly affects the condensation heat transfer due to the thermal resistance through the droplet itself.

$$R_{drop} \sim \left(\frac{3\sigma(\cos(\theta_R) - \cos(\theta_A))}{2\pi\rho g} \right)^{1/2} \tag{S6}$$

This is particularly important for rare earth oxide (REO) surfaces, where the contact angle hysteresis is up to 50–60° and can significantly hinder the shedding of droplets, thus degrading the heat transfer performance.

Supplemental Figures

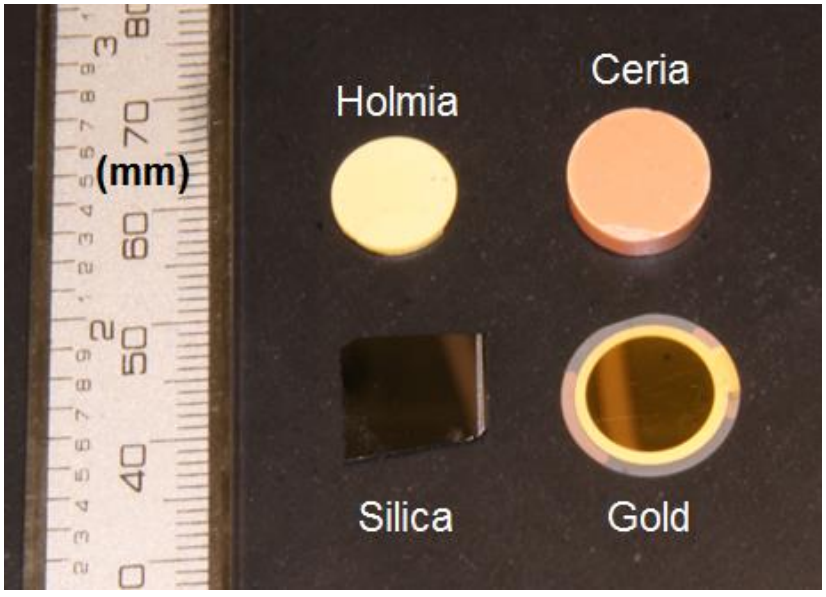

FIG. S1. Image of the samples used for contact angle and XPS measurements. The silica sample is a 100 nm thick silicon dioxide layer on a silicon wafer. The gold sample is a sensor for a quartz crystal microbalance with 100 nm gold deposited on a glass substrate.

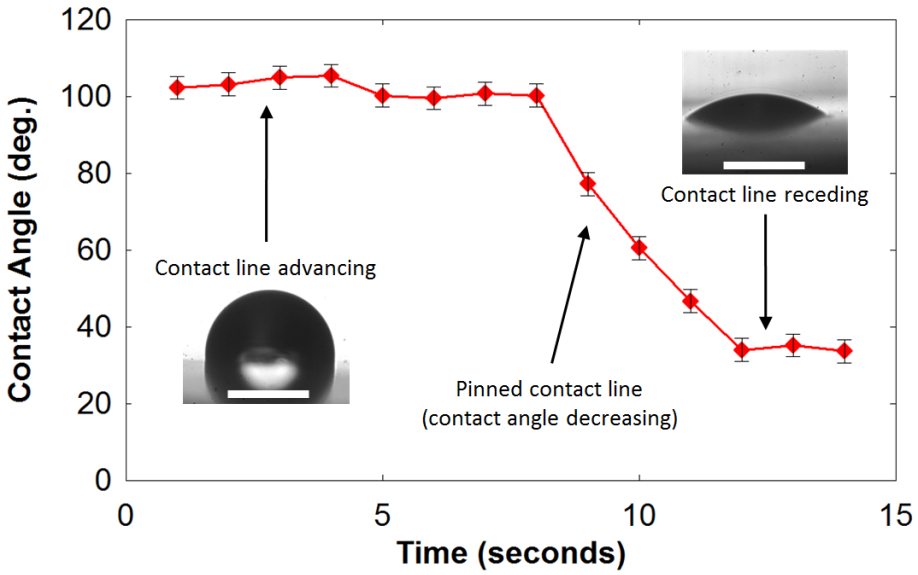

FIG. S2. Representative data for measured contact angle on the holmia sample after exposure to laboratory air (temperature ≈ 25 °C, relative humidity ≈ 35%) for 2448 hr after plasma cleaning the sample. Initially, water was added to the droplet *via* the piezoelectric head on the microgoniometer at a greater rate than the evaporation rate of water from the droplet, and the droplet increased in volume by increasing the perimeter of the contact line at the advancing contact angle. At t = 8 seconds, water addition to the droplet was halted and it immediately began to decrease in volume as evaporation occurred. At first, the decrease in volume manifested as a decrease in the contact angle with a pinned contact line. When the contact angle reached the receding contact angle, the contact angle stopped decreasing and the contact line perimeter decreased, shown here for $t \geq 12$ seconds. Scale bars are 50 μm.

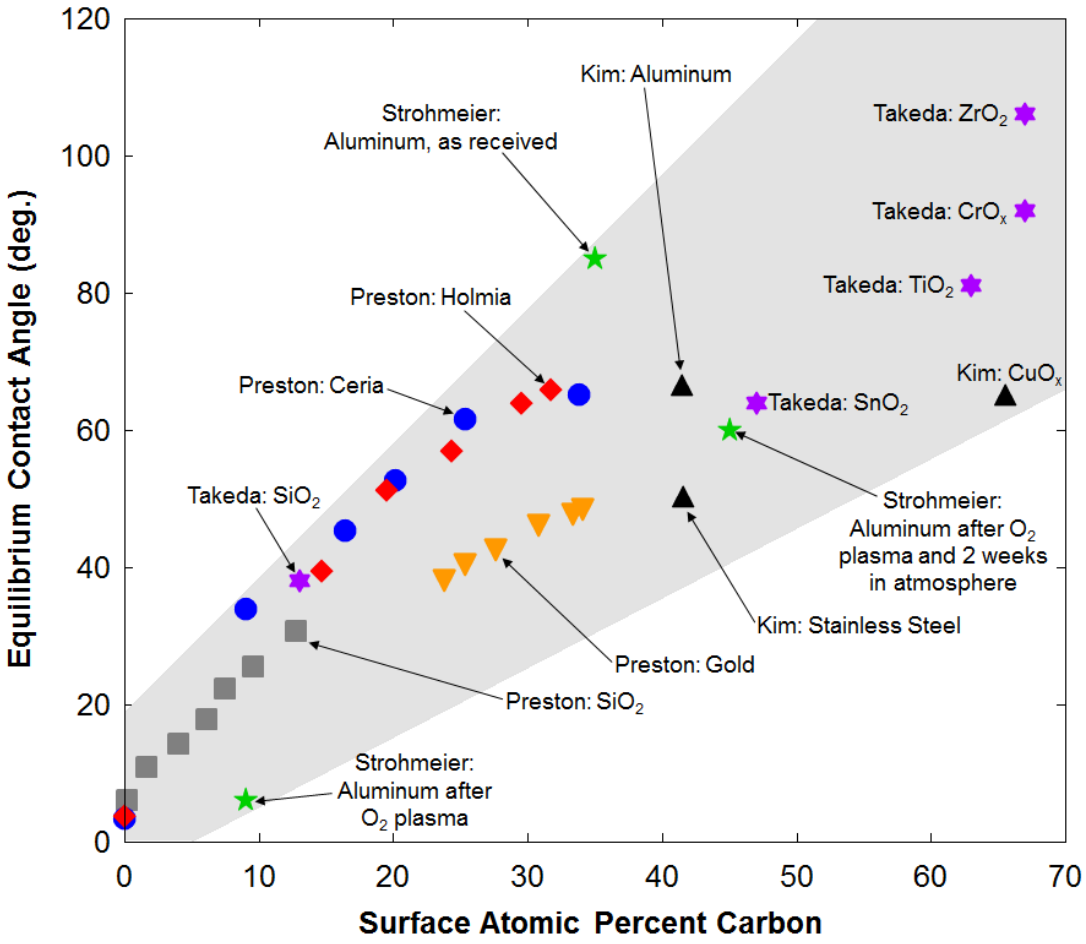

FIG. S3. Comparison of experimental data from the present work (Preston) to previously published results for equilibrium contact angle as a function of surface atomic percent carbon. The previous studies provided only equilibrium contact angles, so the advancing and receding contact angles for the materials studied in the present work were arithmetically averaged to estimate the equilibrium contact angle, which is plotted here for fair comparison. Takeda deposited 40-nm-thick metal oxide films onto a silica substrate by reactive magnetron sputtering and exposed the samples to atmosphere with controlled relative humidity and temperature.[8] Kim provided contact angle and XPS measurements for bare metals which had been exposed to atmosphere for long times.[9] Strohmeier cleaned cold-rolled aluminum foil with oxygen plasma and subsequently exposed the foil to ambient atmosphere (experimental data for as-received bare aluminum was also included).[10] The shaded region highlights the positive correlation between contact angle and surface carbon contamination, which applies to rare earth oxides as well as metals, metal oxides, and silica. The data spread is attributed to differences in hydrocarbon alignment when adsorbed on different materials, preferential adsorption of certain species of hydrocarbons for each material, and the use of surface atomic percent carbon as opposed to surface area fraction of hydrocarbons, which would account for the relative sizes of hydrocarbons versus surface molecules.

Supplemental References

[1] Y. S. Touloukian, (IFI/Plenum, New York, 1970), Vol. 2.

[2] L. Fomarini, J. C. Conde, C. Alvani, D. Olevano, and S. Chiussi, Thin Solid Films **516** (21), 7400 (2008).

[3] M. Mogensen, N. M. Sammes, and G. A. Tompsett, Solid State Ionics **129** (1-4), 63 (2000).

[4] J. J. Martin and G. S. Dixon, Phys Status Solidi B **54** (2), 707 (1972).

[5] K. E. Gilchrist, R. G. Brown, and S. D. Preston, J Nucl Mater **68** (1), 39 (1977).

[6] E. Bormashenko, R. Pogreb, G. Whyman, and M. Erlich, Langmuir **23** (24), 12217 (2007); X. Noblin, A. Buguin, and F. Brochard-Wyart, Eur Phys J E **14** (4), 395 (2004).

[7] F. Celestini and R. Kofman, Phys Rev E **73** (4) (2006).

[8] S. Takeda, M. Fukawa, Y. Hayashi, and K. Matsumoto, Thin Solid Films **339** (1-2), 220 (1999).

[9] M. C. Kim, S. H. Yang, J. H. Boo, and J. G. Han, Surf Coat Tech **174**, 839 (2003).

[10] B. R. Strohmeier, J Vac Sci Technol A **7** (6), 3238 (1989).